Formation of the bi-directional energy cascade in low-frequency damped wave-turbulent systems

2015 EPL 112 24004

(http://iopscience.iop.org/0295-5075/112/2/24004)

A Letters Journal Exploring the Frontiers of Physics

October 2015

EPL, **112** (2015) 24004
doi: 10.1209/0295-5075/112/24004

www.epljournal.org

Formation of the bi-directional energy cascade in low-frequency damped wave-turbulent systems

Yuri V. Lvov[1], Andy He[2] and German V. Kolmakov[2]

[1] *Department of Mathematical Sciences, Rensselaer Polytechnic Institute - Troy, NY 12180, USA*
[2] *Physics Department, New York City College of Technology, City University of New York Brooklyn, NY 11201, USA*

received 13 June 2015; accepted in final form 17 October 2015
published online 4 November 2015

PACS 47.27.-i – Turbulent flows
PACS 68.03.Kn – Dynamics (capillary waves)

Abstract – We demonstrate that in wave-turbulent systems, an inverse energy flux can be formed in addition to the conventional direct energy flux if large-scale wave damping is present. Such a bi-directional energy cascade can be understood in terms of the wave energy transfer on the temperature wave background. The formation of the bi-directional cascade provides an effective mechanism for global coupling between the scales where the turbulent fluctuations at small scales are affected by the wave distribution at large scales due to the total energy conservation. We discuss physical systems where this scenario is realized.

Introduction. – Turbulence appears in many systems ranging from planetary vortices to quantum systems [1–3]. In addition to vortex turbulence familiar to everyone and, probably, first sketched in classic works by Leonardo da Vinci [4], turbulence can also form in a system of waves [2,5]; the latter is termed wave, or weak turbulence. Classic examples of wave turbulence are ensembles of gravity wind-generated surface waves in an open sea [3] and capillary surface waves [6–9]. Wave turbulence also forms in various nonlinear systems including interstellar plasmas [10], optical waveguides [11], phonons in solids [12], Bose-Einstein condensates (BECs) of ultra-cold atoms [13] and of excitons in semiconductors [14], interacting sound waves in superfluid liquids [15], and vibrating plates [16], to name a few.

A wave-turbulent ensemble is described by the kinetic equation [2,5]

$$\frac{\partial n(\boldsymbol{k})}{\partial t} = \mathrm{St}[n(\boldsymbol{k})] + \Gamma(\boldsymbol{k}), \tag{1}$$

where the nonlinear dynamics for the pair correlation function for wave amplitudes in the K-representation, $n(\boldsymbol{k})$, is captured by the collision integral $\mathrm{St}[n(\boldsymbol{k})]$, and $\Gamma(\boldsymbol{k})$ accounts for the energy injection ($\Gamma(\boldsymbol{k}) > 0$) and damping ($\Gamma(\boldsymbol{k}) < 0$). In analogy with vortex turbulence [1], the wave turbulence dynamics is controlled by fluxes of the integrals of motions of the underlying physical systems [2,5]. For decaying waves ($\partial^2\omega(\boldsymbol{k})/\partial\boldsymbol{k}^2 > 0$, where $\omega(\boldsymbol{k})$ is a linear dispersion relation with $\boldsymbol{k}$ to be a wave vector), the only integral of motion of eq. (1) is the wave energy. The respective steady state is the direct Zakharov spectrum, which carries the wave energy through the scales from the pumping scales towards the small-scale domain [2,5].

It has recently been found in experiments with capillary waves on the fluid surface [17] and with nonlinear sound waves in superfluid helium [15] that, in contrast to the conventional wisdom, under certain conditions the energy in the turbulent spectrum can simultaneously flow to the high- and low-frequency spectral domains from the pumping scales. In other words, a *bi-directional energy cascade* can form in a nonlinear wave system. However, despite these observations are supported by direct numerical modeling of the specific systems [15,17], the reason for a bi-directional energy cascade formation has not yet been clearly understood. The formation of a bi-directional energy cascade has been recently observed also in direct numerical simulations of vortex turbulence [18,19].

In this paper, we show that a bi-directional energy cascade can be understood as a perturbation of the thermal Rayleigh-Jeans distribution at low frequencies, whereas at high frequencies it coincides with Zakharov direct cascade. It is found that the bi-directional energy cascade forms if wave damping is presented in both high- and low-frequency domains.

When low-frequency damping is presented, the respective low-frequency wave amplitudes are suppressed and an inverse energy flux towards the low-frequency domain is formed to restore the thermodynamic equilibrium at frequencies lower than the pump frequency.

Bi-directional cascade in scale-invariant wave systems. – For waves with the decay dispersion law, the collision integral reads [2,5]

$$\mathrm{St}[n(\boldsymbol{k})] = \int \mathrm{d}^d\boldsymbol{k}_1\mathrm{d}^d\boldsymbol{k}_2[R(\boldsymbol{k},\boldsymbol{k}_1,\boldsymbol{k}_2) - R(\boldsymbol{k}_1,\boldsymbol{k},\boldsymbol{k}_2) - R(\boldsymbol{k}_1,\boldsymbol{k}_2,\boldsymbol{k})], \quad (2)$$

where $R(\boldsymbol{k},\boldsymbol{k}_1,\boldsymbol{k}_2) = \pi|V(\boldsymbol{k},\boldsymbol{k}_1,\boldsymbol{k}_2)|^2\delta(\boldsymbol{k}-\boldsymbol{k}_1-\boldsymbol{k}_2)\delta(\omega(\boldsymbol{k})-\omega(\boldsymbol{k}_1)-\omega(\boldsymbol{k}_2)[n(\boldsymbol{k}_1)n(\boldsymbol{k}_2)-n(\boldsymbol{k})(n(\boldsymbol{k}_1)+n(\boldsymbol{k}_2))]$, $V(\boldsymbol{k},\boldsymbol{k}_1,\boldsymbol{k}_2)$ is the matrix element of the wave interaction, Dirac deltas account for the conservation of the linear momentum (wave vector) and the energy (frequency), d is the dimensionality of space.

In many systems, the frequency and the interaction matrix elements are scale-invariant functions

$$\omega(\lambda\boldsymbol{k}) = \lambda^\alpha\omega(\lambda\boldsymbol{k}),$$
$$V(\lambda\boldsymbol{k},\lambda\boldsymbol{k}_1,\lambda\boldsymbol{k}_2) = \lambda^m V(\boldsymbol{k},\boldsymbol{k}_1,\boldsymbol{k}_2), \quad (3)$$

where λ is a dilatation factor, and α and m are the respective scaling indices. In this case the kinetic wave equation, eqs. (1) and (2), has a steady-state scale-invariant turbulent solution, Zakharov spectrum,

$$n(\boldsymbol{k}) = CP^{1/2}k^{-s}, \quad (4)$$

where P is the energy flux, C is the positive Kolmogorov constant, and $s = d + m$ is the scaling index [2]. The spectrum (4) is formed in the inertial range of frequencies ($\Gamma(\boldsymbol{k}) = 0$). Since $P > 0$, the spectrum (4) carries the energy flux towards the high-frequency spectral domain and hence, it forms at frequencies higher than a characteristic energy pump frequency. The spectrum (4) is a wave analogue of the Kolmogorov spectrum of vortex turbulence [1].

For an ideal, non-dissipative system, an equilibrium Rayleigh-Jeans spectrum

$$n_{\mathrm{eq}}(\boldsymbol{k}) = \frac{T}{\omega(\boldsymbol{k})} \quad (5)$$

is established at the scales larger than the energy injection scale with T to be the effective temperature [20]. In most systems, one has $s/\alpha > 1$ thus, the turbulent solution decays faster than the equilibrium one with growing wave vector $\boldsymbol{k}$.

A general form of the wave distribution can be restored from the dimensional arguments that gives [2]

$$n(\boldsymbol{k}) = \frac{T}{\omega_k}g\left[P\left(\frac{C\omega_k}{Tk^s}\right)^2\right], \quad (6)$$

where the function $g(x) = 1 + c_1x$ at $x \to 1$ and $g(x) \propto x^{1/2}$ at $x \to \infty$, where c_1 is a constant. By using the Kraichnan-Zakharov conformal mapping $k^2/k_1 \to k_1$, $kk_2/k_1 \to k_2$ in the second term in the integral in eq. (2) and $kk_2/k_1 \to k_1$ and $k^2/k_1 \to k_2$ in the third term in the integral, one can show that, in a system close to equilibrium (*i.e.*, for a small flux P), the steady-state distribution, eq. (6), reads

$$n(\boldsymbol{k}) = \frac{T}{\omega(\boldsymbol{k})} + \text{const } Pk^{\alpha-2(m+d)}. \quad (7)$$

We note that, in contrast to eq. (4), in the perturbed thermal distribution (7) the flux P can be positive or negative and then, the wave energy can propagate in both directions.

Differential approximation. – It follows from the kinetic equation (1) that in the inertial range the wave energy density in K-space, $E(\boldsymbol{k}) = \pi(2k)^{d-1}\omega(\boldsymbol{k})n(\boldsymbol{k})$, obeys the continuity equation

$$\frac{\partial E(\boldsymbol{k})}{\partial t} + \frac{\partial P}{\partial k} = 0. \quad (8)$$

In what follows we consider isotropic turbulence. If the integral $\mathrm{St}[n(\boldsymbol{k})]$ converges, the expression for the energy flux can be approximated as a differential operator that yields the results, which are in a good agreement with the "exact" theory or direct numerical simulations [8,11,21,22]. In this approximation, the energy flux is the following:

$$P = -a\omega^{\frac{2(d+m)}{\alpha}}n_\omega\frac{\partial}{\partial\omega}(\omega n_\omega), \quad (9)$$

where a is a positive constant. From eqs. (8) and (9) it follows that the isotropic wave distribution obeys the kinetic equation

$$\frac{\partial n_\omega}{\partial t} = \frac{1}{\omega^{\frac{d}{\alpha}}}\frac{\partial}{\partial\omega}\left[n_\omega\omega^{\frac{2(d+m)}{\alpha}}\frac{\partial}{\partial\omega}(\omega n_\omega)\right] + \Gamma(\omega). \quad (10)$$

Here, we normalized time by the dimensional constant, $t \to a^{-1}t$, so that we set $a = 1$. We also expressed the wave distribution via the frequency ω with the help of the dispersion relation, $n_\omega = n(\boldsymbol{k})|_{k=k(\omega)}$. The first term in the right-hand side of eq. (10) presents the differential approximation of the "full" collision integral $\mathrm{St}[n(\boldsymbol{k})]$ in eq. (1). The spectra (4) and (5) are solutions of the steady-state equation (10) in the inertial range of frequencies. Equation (10) predicts the same frequency dependence of the characteristic turbulent relaxation time as the exact kinetic equation, $\tau(\omega) \propto \omega^{1-\frac{2m+d}{\alpha}}n_\omega^{-1}$. The Kolmogorov constant estimated from eq. (9) is $C = (s/\alpha - 1)^{-1/2}$. For instance, for capillary waves ($d = 2$, $\alpha = 3/2$, $m = 9/4$ [2]), this gives $C = \sqrt{6/11} \approx 0.74$.

The steady-state solution of eq. (10) in the inertial range, $\Gamma(\omega) = 0$, is

$$n_\omega = \omega^{-1}\sqrt{T^2 + C^2P\omega^{2(1-\frac{s}{\alpha})}}. \quad (11)$$

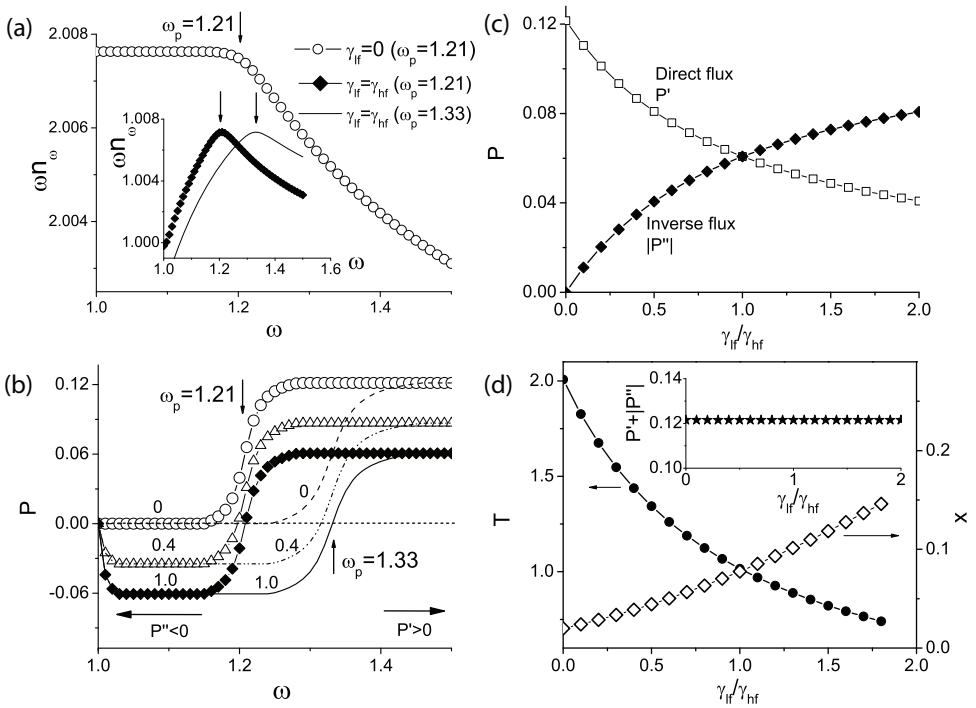

Fig. 1: Formation of a bi-directional energy cascade of capillary waves with rising the low-frequency damping coefficient from $\gamma_{lf} = 0$ to $\gamma_{lf} = \gamma_{hf}$. (a) Main plot: the compensated spectrum ωn_ω numerically calculated from eq. (10) for $\gamma_{lf} = 0$, $\omega_p = 1.21$ and $\gamma_p = \gamma_{hf} = 1$ in the used dimensionless units. Inset: the compensated spectra with $\gamma_{lf}/\gamma_{hf} = 1$ for $\omega_p = 1.21$ (points) and for $\omega_p = 1.33$ (a solid curve). In the simulations, the data were discretized in u-scale; we used the predictor-corrector Adams method with the maximum number of numerical points of 200. (b) The energy flux, eq. (9), as a function of the wave frequency ω, calculated from n_ω. Points: $\omega_p = 1.21$; curves: $\omega_p = 1.33$. The numbers at the curves show the respective value of γ_{lf}/γ_{hf}. Lines connecting the points are shown to guide the eye. The plateaus in (b) correspond to the formation of a constant direct energy flux ($P' > 0$) at $\omega > \omega_p$ and of an inverse energy flux ($P'' < 0$) at $\omega < \omega_p$. (c) Dependence of the direct energy flux, P', and of the inverse energy flux, $|P''| \equiv -P''$, on the low-frequency damping coefficient γ_{lf} for $\omega_p = 1.21$. The inverse flux $P'' \neq 0$ builds up if $\gamma_{lf} > 0$. The inset in (d) shows the total energy flux $P' + |P''|$ outcoming from the pumping spectral domain. Independence of the total flux on low-frequency damping reflects the energy conservation in the wave system. (d) Main plot (filled circles, left scale): dependence of the effective temperature T of low-frequency turbulent distribution on γ_{lf} obtained by fitting of the numerical spectrum n_ω with eq. (11). Unfilled diamonds, right scale: dependence of the dimensionless parameter x, eq. (14), on γ_{lf}/γ_{hf} for $\omega_p = 1.21$.

It reproduces the equilibrium spectrum (5) for $P = 0$ and the turbulent spectrum (4) at $T = 0$. For small flux P, the spectrum can be found by expanding (11), that gives

$$n_\omega \approx \frac{T}{\omega} + \left(\frac{C^2 P}{T}\right)\omega^{1-\frac{2s}{\alpha}}. \qquad (12)$$

This expansion coincides with the solution (7) obtained for the full kinetic equation (1).

To characterize the conditions, under which the bi-directional cascade can be formed, we numerically studied the wave kinetic equation (10). For this purpose, the steady-state equation (10) ($\dot{n}_\omega = 0$) was rewritten in the variables $f = (\omega n_\omega)^2$, $u = \omega^{-2/C^2}$ as follows:

$$f_{uu} + \gamma^{(d)}(u) f^{1/2} = \gamma^{(p)}(u), \qquad (13)$$

where the subscript u denotes the derivative, $\gamma_d(u)$ describes linear wave damping and $\gamma_p(u)$ accounts for the wave energy pump. We normalize the wave frequency to the minimum frequency in the system, $\omega/\omega_{min} \to \omega$; the dimensionless frequency range $\omega \in [1, +\infty)$ is mapped to the range $u \in (0, 1]$. In what follows, we consider a model when the pump term and the low- and high-frequency damping terms are described by a normalized Lorentzian function $L(u, u_0) = \Delta u^2/[(u - u_0)^2 + \Delta u^2]$ centered in the middle and at the edges of the inertial range, respectively, $\gamma^{(p)}(u) = \gamma_p L(u, u_p)$, $\gamma^{(d)}_{lf}(u) = \gamma_{lf} L(u, 1)$, and $\gamma^{(d)}_{hf}(u) = \gamma_{hf} L(u, 0)$, with γ_p and u_p to be the pump rate and scale ($0 < u_p < 1$), and γ_{lf} and γ_{hf} to be the low- and high-frequency damping coefficients. The total damping was represented by a sum of low- and high-frequency damping, $\gamma^{(p)}(u) = \gamma^{(d)}_{lf}(u) + \gamma^{(d)}_{hf}(u)$, and the width of the Lorentzian function was taken equal to a small value $\Delta u = 0.025$. Equation (13) has been numerically solved with zero-flux boundary conditions at the edges of the numerical interval, $f_u(0) = f_u(1) = 0$.

Figure 1(a) (points) shows the result of the numerical solution of eq. (13) for capillary waves shown in ω-scale

for the pump frequency $\omega_p = u_p^{-C^2/2} \approx 1.21$ in units of ω_{min}. It is seen that, if low-frequency damping is absent ($\gamma_{lf} = 0$), the obtained numerical solution represents the thermal spectrum $\omega n_\omega = const \equiv T$ at $\omega < \omega_p$ in agreement with refs. [17,20]. At high frequencies, $\omega > \omega_p$, a conventional direct-flux Zakharov solution (4) is formed. In the presence of low-frequency damping, $\gamma_{lf}/\gamma_{hf} = 1$, the compensated wave spectrum ωn_ω is as a hump-like function with the maximum positioned at $\omega = \omega_p$.

Figure 1(b) shows the energy flux calculated with eq. (9) from the numerical spectrum n_ω for three different values of γ_{lf}. It is seen that in the high-frequency inertial range $\omega > \omega_p$, the energy flux is equal to a positive constant value that corresponds to establishment of the direct wave-turbulent cascade in the system. In the presence of low-frequency damping, $\gamma_{lf} > 0$, a constant, *negative* energy flux is also formed in the low-frequency inertial range $\omega < \omega_p$. This negative flux carries the wave energy from the pump scales towards the low-frequency scales where it is absorbed by low-frequency damping. In other words, the bi-directional energy cascade is established if wave damping is present at both the low and high frequencies. We will denote the energy fluxes towards the high- and low-frequency domains as $P' > 0$ and $P'' < 0$, respectively, as marked in fig. 1(b) by horizontal arrows.

Figure 1(c) shows the magnitudes of the direct and inverse fluxes calculated from the data similar to those shown in fig. 1(b) as functions of the low-frequency damping coefficient γ_{lf}; all other parameters are kept fixed. It is seen that the inverse flux $|P''|$ is increased with rising γ_{lf} (filled diamonds). At the same time, the direct energy flux P' is decreased (unfilled squares). The total energy flux $P \equiv P' + |P''|$ carried out from the pump frequency is constant (inset in fig. 1(d)), that reflects the energy conservation in the system.

We also determined the effective temperature T of the low-frequency wave distribution ($\omega < \omega_p$) by fitting the numerical results for n_ω with eq. (11). The dependence of T on low-frequency damping is show in the main plot of fig. 1(d) (left scale). It is seen that the effective temperature is a decreasing function of the damping coefficient γ_{lf}. This can be understood as follows. Wave turbulence is characterized by fluctuations of the wave amplitudes at a given frequency, A_ω, with the probability $w(A_\omega) \propto \exp(-|A_\omega|^2/2n_\omega)$ [23]. Additional damping results in the decrease of the wave amplitudes (see fig. 1(a)) and hence, in smaller fluctuations of the wave amplitudes about the mean. The decrease of the fluctuations can be considered as an effective "cooling" of the wave system.

We found that whereas the steady-state distribution n_ω depends on the pump frequency, the fluxes P' and P'' and the temperature T at $\omega < \omega_p$ do not depend on the pump frequency and are only controlled by damping at the edges of the inertial range. While the distribution n_ω changes with increasing pump frequency from $\omega_p = 1.21$ (filled diamonds) to $\omega_p = 1.33$ (a solid curve in fig. 1(a)), the energy fluxes P' and P'' at the plateaus on the $P(\omega)$ curve remain the same within the accuracy of the simulations $\leq 0.3\%$ (fig. 1(b), curves). The effective temperature T was also unchanged within the same accuracy of $\leq 0.3\%$ after ω_p was changed from 1.21 to 1.33.

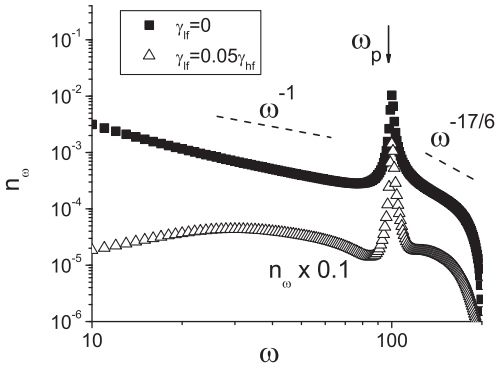

Fig. 2: Evolution of the steady-state capillary-wave spectrum with rising low-frequency damping from $\gamma_{lf} = 0$ to $\gamma_{lf} = 0.05\gamma_{hf}$ calculated from the full kinetic equation, eqs. (1) and (2). To make the data more visible, the spectrum n_ω for $\gamma_{lf} = 0.05\gamma_{hf}$ is reduced by the factor of ten. The dashed lines show the thermal Rayleigh-Jeans spectrum $n_\omega \propto \omega^{-1}$ and Zakharov spectrum $n_\omega \propto \omega^{-17/6}$. It is seen that the spectrum deviates from the thermodynamic equilibrium $n_\omega \propto \omega^{-1}$ as low-frequency damping grows. The data were obtained by iteratively solving the steady-state kinetic equation $\mathrm{St}[n(\boldsymbol{k})] + \Gamma(\boldsymbol{k}) = 0$ in the spectral domain $\omega_{min} \leq \omega \leq \omega_{max}$ where $\omega_{min} = 1$ and $\omega_{max} = 200$ in the used numerical units. The source-damping term was set equal to $\Gamma(\boldsymbol{k}) = \gamma^{(p)}(\omega(k)) - \gamma^{(d)}(\omega(k))n_\omega$. Pumping was modeled as $\gamma^{(p)}(\omega) = \gamma_p L(\omega, \omega_p)$ with the pump frequency $\omega_p = 100\omega_{min}$. Total linear damping was set equal to a sum of low- and high-frequency Lorentzian-shaped damping terms, $\gamma^{(d)}(\omega) = \gamma^{(d)}_{lf}(\omega) + \gamma^{(d)}_{hf}(\omega)$, where $\gamma^{(d)}_{lf}(\omega) = \gamma_{lf} L(\omega, \omega_{min})$ for $\omega < \omega_p$ and $\gamma^{(d)}_{hf}(\omega) = \gamma_{hf} L(\omega, \omega_{max})$ for $\omega > \omega_p$ with γ_{lf} and γ_{hf} to be the low- and high-frequency damping coefficients. The width of the Lorentzian function was set as $\Delta\omega = \omega_{min}$; the matrix element in eq. (2) was taken equal to $V(\boldsymbol{k}, \boldsymbol{k}_1, \boldsymbol{k}_2) = \varepsilon\sqrt{\omega(k)\omega(k_1)\omega(k_2)}$ with the dimensionless nonlinearity $\varepsilon = 2 \times 10^{-3}$ [17]; the pumping rate and the high-frequency damping coefficient were kept fixed throughout the simulations, $\gamma_p = 10^{-2}$ and $\gamma_{hf} = 10^3$. The numerical points were evenly distributed in ω-space. The accuracy of the solution determined as a change of the compensated spectrum ωn_ω after one iteration is better than 1.5×10^{-5}, the relative accuracy for the compensated spectrum is better than 2×10^{-6}.

The wave distribution can be characterized by the dimensionless parameter

$$x = C^2(P' + |P''|)\omega_p^{2(1-\frac{s}{\alpha})}T^{-2}. \qquad (14)$$

Dependence of x on the ratio γ_{lf}/γ_{hf} for $\omega_p = 1.21$ is shown in fig. 1(d) (right scale). It is seen that x is increased from ~ 0.02 for $\gamma_{lf} \ll \gamma_{hf}$ to ~ 0.15 at $\gamma_{lf} = 1.8\gamma_{hf}$. Thus, the relative contribution of the energy flux to the over-all wave distribution grows

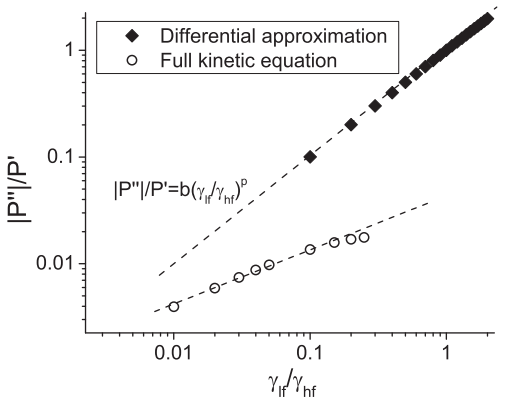

Fig. 3: Inverse-to-direct flux ratio $|P''|/P'$ *vs.* the ratio of the low- and high-frequency damping coefficients. Filled diamonds: the differential approximation (eq. (10) and fig. 1); unfilled circles: the full kinetic equation for the capillary wave (eqs. (1) and (2) and fig. 2). The inverse energy flux towards the low-frequency domain builds up with the growth of low-frequency wave damping. For the full kinetic equation, the fluxes were calculated as $P' = \int_{\omega_p}^{\omega_{max}} \mathrm{d}\omega\gamma(\omega)E(\omega)$, $P'' = -\int_{\omega_{min}}^{\omega_p} \mathrm{d}\omega\gamma(\omega)E(\omega)$, where $E(\omega) = (\mathrm{d}k(\omega)/\mathrm{d}\omega)E(k(\omega))$ is the energy density in ω-space, $k(\omega)$ is a function inverse to the dispersion relation [2,17]; the domain $|\omega - \omega_p| \leq 10\Delta\omega$ was excluded from the integration to ignore the effect of the direct pumping on the flux. The numerical data can be fitted by a power-like function $|P''|/P' = b(\gamma_{lf}/\gamma_{hf})^p$ (dashed lines). The fitting coefficients depend on the system parameters, in agreement with ref. [17]; $b \approx 0.998$ and $p \approx 0.995$ for the differential approximation and $b \approx 0.240$ and $p \approx 0.467$ for the full kinetic equation.

with increasing low-frequency damping, in agreement with above consideration.

Kinetic equation. – To further understand the inverse energy flux formation, we studied the wave dynamics with the full kinetic equation, eqs. (1) and (2). In the simulations, Lorentzian-shaped damping was applied at both edges of the numerical interval $[\omega_{min}, \omega_{max}]$, and pumping was positioned at the center of the interval. The steady-state turbulent spectra without low-frequency damping ($\gamma_{lf} = 0$) and with low-frequency damping ($\gamma_{lf} > 0$) are shown in fig. 2. It is seen that, if low-frequency damping is absent ($\gamma_{lf} = 0$, filled squares), Zakharov and Rayleigh-Jeans distributions, eqs. (4) and (5), are reproduced in the low- and high-frequency domains, respectively. With the increase of the low-frequency damping ($\gamma_{lf} > 0$, unfilled triangles), the low-frequency spectrum deviates from the Rayleigh-Jeans asymptotics, in agreement with the above consideration (fig. 1(a)).

To compare the results obtained for the differential approximation (see the section above) and for the full kinetic equation (this section), we show in fig. 3 the dependence of the dimensionless ratio $|P''|/P'$ on the ratio of the low- and high-frequency damping coefficients γ_{lf}/γ_{hf}. It is seen in fig. 3 that in both cases, this dependence can be approximated as a power-like function $|P''|/P' = b(\gamma_{lf}/\gamma_{hf})^p$ with the pre-exponent b and the exponent p to be functions of the parameters of the system; the latter is in agreement with the results of direct numerical simulations of the surface wave dynamics, ref. [17].

Discussion and outlook. – From the above consideration it follows that the bi-directional energy cascade can form in the wave-turbulent system if damping is presented at both low- and high-frequency scales. In actual physical hydrodynamic-type systems, high-frequency damping is usually associated with the viscous losses in the bulk or at the surface of the systems [1,2]. The reasons for the low-frequency damping depend on the specifics of the system. For instance, for capillary surface waves in a vessel, the low-frequency damping originates from the viscous drag at the bottom or at the vertical walls of the vessel [24]. In Bose-Einstein condensates of ultra-cold atoms, the effective damping is caused by the condensate depletion due to evaporation of the atomic cloud. For turbulent Bose-Einstein condensates of excitons in planar semiconductor heterostructures [14] the effective damping is caused by the finite lifetime of excitons due to the electron-hole recombination.

The formation of the inverse energy cascade can probably result in the modification of the inverse wave action cascade existing in the systems with the non-decay dispersion relations, *e.g.*, for long, gravity surface waves on the ocean surface [3]. In the latter case, the low-frequency cascade is terminated by breaking waves that provides a nonlinear alternative to wave damping. In other words, the large length scale absorption mechanisms for the wave action and the inverse energy cascades are physically the same. This might impose a general constraint for the magnitudes of the inverse energy and wave action fluxes. A similar question on the interference of the two inverse cascades arises for weak (dilute) BECs [13,25,26] where the inverse wave action cascade is formed due to the approximate conservation of the total number of the condensate particles.

In the case of turbulence of second sound (*i.e.*, weakly dissipative thermal waves) in superfluid helium He-II in a cryoacoustic waveguide, the low-frequency damping originates from the viscous drag of the normal component of the superfluid liquid at the waveguide's walls [15]. The conditions of low-frequency wave generation have been considered in [15]. However, it is known [2] that the scenario for turbulence development in acoustic systems is different from that for dispersive waves —formation of strongly anisotropic, interacting shock waves instead of Zakharov spectrum formation.

Since the differential approximation also presents a reliable model for Kelvin wave turbulence, which is quantized vortex turbulence in superfluid liquids at low temperatures [27,28], our findings can be applied to this system —however, also with some reservations. Specifically, the presence of the inverse cascade in this system results in

interesting physics where a bi-directional energy cascade might interfere with a flux of the wave action for the oscillations of the quantum vortex cores. Additionally, the energy losses due to sound emission by Kelvin waves are effective at all length scales [27] that should also lead to the modification of the obtained results.

Conclusions. – Summarizing, we demonstrate that the bi-directional energy cascade can be understood in terms of the wave turbulence theory as the formation of the direct and inverse energy fluxes on the temperature wave background. It is shown that the account for wave damping at large wave length scales is of key importance in the description of the bi-directional cascade. The effective temperature of the wave system at low frequencies is a function of the wave damping coefficient and the temperature decreases when the bi-directional cascade builds up. The formation of the bi-directional cascade provides an effective mechanism for global coupling between the scales where the turbulent fluctuations at small scales are affected by wave damping at large scales due to the total energy conservation.

The obtained results can be applied to various physical systems, for instance, to those mentioned in the "Discussion and outlook" section. In the paper, we considered the case where the wave energy is the only conserving integral of motion. It is also of importance to understand how the inverse energy cascade can interfere with the inverse wave action cascade existing in the systems with more than one integral of motion, *e.g.*, weak Bose-Einstein condensates [13,26], surface gravity waves on the ocean surface [3] and interacting sound waves in superfluid liquids [29]. Since the bi-directional energy cascade can only form on the thermal background, the role of temperature fluctuations should also be explored for such systems.

* * *

The authors are grateful to the Center for Theoretical Physics at New York City College of Technology of the City University of New York for providing computational resources. GVK gratefully acknowledges support from the Professional Staff Congress —City University of New York award #67143-0045. AH and GVK are grateful to Army Research Office, grant #64775-PH-REP, for partial support.

REFERENCES

[1] Frisch U., *Turbulence* (Cambridge University Press, Cambridge) 1995.
[2] Zakharov V. E., L'vov V. S. and Falkovich G., *Kolmogorov Spectra of Turbulence I* (Springer, Berlin) 1992.
[3] Zeitlin V., *Wave turbulence with applications to atmospheric and oceanic waves*, in *Nonlinear Waves in Fluids: Recent Advances and Modern Applications*, edited by Grimshaw R., *CISM International Centre for Mechanical Sciences Series*, Vol. **483** (Springer, Vienna) 2005, pp. 135–168.
[4] Richter J. P., *The Notebooks of Leonardo da Vinci* (Dover, New York) 1970.
[5] Nazarenko S., *Wave Turbulence* (Springer-Verlag, Heidelberg) 2011.
[6] Wright W. B., Budakian R. and Putterman S. J., *Phys. Rev. Lett.*, **76** (1996) 4528.
[7] Henry E., Alstrom P. and Levinsen M. T., *Europhys. Lett.*, **52** (2000) 27.
[8] Kolmakov G. V., Levchenko A. A., Brazhnikov M. Y., Mezhov-Deglin L. P., Silchenko A. N. and McClintock P. V. E., *Phys. Rev. Lett.*, **93** (2004) 074501.
[9] Falcon E., Laroche C. and Fauve S., *Phys. Rev. Lett.*, **98** (2007) 094503.
[10] Scarf F. L., Gurnett D. A. and Kurth W. S., *Nature*, **292** (1981) 747.
[11] Dyachenko S., Pushkarev A. and Zakharov V. E., *Physica D*, **57** (1992) 96.
[12] Tsoi V. S., *Cent. Eur. J. Phys*, **1** (2003) 72.
[13] Zakharov V. E. and Nazarenko S. V., *Physica D*, **201** (2005) 203.
[14] Berman O. L., Kezerashvili R. Y., Kolmakov G. V. and Lozovik Y. E., *Phys. Rev. B*, **86** (2012) 045108.
[15] Ganshin A. N., Efimov V. B., Kolmakov G. V., Mezhov-Deglin L. P. and McClintock P. V. E., *Phys. Rev. Lett.*, **101** (2008) 065303.
[16] Cobelli P., Petitjeans P., Maurel A., Pagneux V. and Mordant N., *Phys. Rev. Lett.*, **103** (2009) 204301.
[17] Abdurakhimov L. V., Arefin M., Kolmakov G. V., Levchenko A. A., Lvov Y. V. and Remizov I. A., *Phys. Rev. E*, **91** (2015) 023021.
[18] Celani A., Musacchio S. and Vincenzi D., *Phys. Rev. Lett.*, **104** (2010) 184506.
[19] Boffetta G., De Lillo F. and Musacchio S., *Phys. Rev. E*, **83** (2011) 066302.
[20] Balkovsky E., Falkovich G., Lebedev V. and Shapiro I. Y., *Phys. Rev. E*, **52** (1995) 4537.
[21] Connaughton C., Newell A. C. and Pomeau Y., *Physica D*, **184** (2003) 64.
[22] Boffetta G., Celani A., Dezzani D., Laurie J. and Nazarenko S., *J. Low Temp. Phys.*, **156** (2009) 193.
[23] Choi Y., Lvov Y. V. and Nazarenko S., *Phys. Lett. A*, **332** (2004) 230.
[24] Christiansen B., Alstrom P. and Levinsen M. T., *J. Fluid Mech.*, **291** (1995) 323.
[25] Dyachenko A. and Falkovich G., *Phys. Rev. E*, **54** (1996) 5095.
[26] Lvov Y., Nazarenko S. and West R., *Physica D*, **184** (2003) 333.
[27] Nazarenko S., *JETP Lett.*, **83** (2006) 198.
[28] Walmsley P. M., Golov A. I., Hall H. E., Levchenko A. A. and Vinen W. F., *Phys. Rev. Lett.*, **99** (2007) 265302.
[29] Kolmakov G. V. and Pokrovsky V. L., *Physica D*, **86** (1995) 456.